Mon. Not. R. Astron. Soc. **000**, 1–?? (2005) Printed 4 September 2008 (MN LATEX style file v2.2)

Detection of the 2175 Å extinction feature and 21-cm absorption in two Mg II systems at $z \sim 1.3$

R. Srianand[1⋆], N. Gupta[2], P. Petitjean[3], P. Noterdaeme[3] and D. J. Saikia[4]
[1] *IUCAA, Post Bag 4, Ganeshkhind, Pune 411 007, India*
[2] *ATNF, CSIRO, P. O. Box 76, Epping, NSW 1710, Australia*
[3] *UPMC Paris 6, Institut d'Astrophysique de Paris, UMR7095 CNRS, 98bis Boulevard Arago, 75014, Paris, France*
[4] *NCRA, Post Bag 3, Ganeshkhind, Pune 411 007, India*

Accepted. Received; in original form

ABSTRACT

We have discovered two dusty intervening Mg II absorption systems at $z \sim 1.3$ in the Sloan Digital Sky Survey (SDSS) database. The overall spectra of both QSOs are red (u-K>4.5 mag) and are well modelled by the composite QSO spectrum reddened by the extinction curve from the Large Magellanic Cloud(LMC2) Supershell redshifted to the rest-frame of the Mg II systems. In particular, we detect clearly the presence of the UV extinction bump at $\lambda_{\rm rest} \sim 2175$ Å. Absorption lines of weak transitions like Si IIλ1808, Cr IIλ2056, Cr II+Zn IIλ2062, Mn IIλ2594, Ca IIλ3934 and Ti IIλ1910 from these systems are detected even in the low signal-to-noise ratio and low resolution SDSS spectra, suggesting high column densities of these species. The depletion pattern inferred from these absorption lines is consistent with that seen in the cold neutral medium of the LMC. Using the LMC A_V vs. N(H I) relationship we derive N(H I)$\sim 6\times10^{21}$ cm^{-2} in both systems. Metallicities are close to solar. Giant Metrewave Radio Telescope (GMRT) observations of these two relatively weak radio loud QSOs ($f_\nu \sim$ 50 mJy) resulted in the detection of 21-cm absorption in both cases. We show that the spin temperature of the gas is of the order of or smaller than 500 K. These systems provide a unique opportunity to search for molecules and diffuse interstellar bands at $z > 1$.

Key words: quasars: active – quasars: absorption lines – quasar: individual : J085042.21+515911.7 - J085244.74+343540.46

1 INTRODUCTION

Studying the physical conditions in the interstellar medium (ISM) at high redshift and the processes that maintain these conditions is important for our understanding of how galaxies form and evolve. The presence of dust influences the physical state of the gas through photo-electric heating, UV shielding, and formation of molecules on the surface of grains. However, we know very little about dust properties in the ISM at high redshifts. Properties of the dust can be derived from extinction curves observed in different astrophysical objects. Recently, Noll et al. (2007) found evidence for the presence of a moderate UV bump in at least part of the population of massive galaxies at $z > 1$. Studies of dust extinction in the circum-burst environment of Gamma Ray Bursts indicate that in most cases, a LMC-like extinction curve is preferred (e.g. Heng et al. 2008).

The depletion of Cr with respect to Zn in intervening damped Lyman-α systems (DLAs) shows that dust is indeed an important component of the high density gas (Pettini, Smith & Hunstead 1994). A correlation is observed in DLAs between metallicity and dust-depletion (Ledoux, Petitjean & Srianand 2003) which is confirmed by the higher detection rate of H_2 in DLAs with higher metallicities (Petitjean et al. 2006; Noterdaeme et al. 2008). The corresponding gas is cold (T∼150 K; Srianand et al. 2005) as expected from multiphase ISM models in which the gas with high metallicity and dust content has lower kinetic temperature than the gas with lower metallicity and dust content (Wolfire et al. 1995). However, even in the highest metallicity DLAs typical dust signatures like high extinction (i.e 0.16≤ E(B−V)≤0.40), 2175 Å absorption bump or the diffuse interstellar bands (DIBs) are not seen.

Signatures of dust are seen from few intermediate and low redshift absorption systems. Both DIBs and 2175Å absorption bump have been detected in the $z_{\rm abs} = 0.524$ system

⋆ E-mail: anand@iucaa.ernet.in

Table 1. GMRT observation log and results

Source name	Date	Time (hr)	Peak Flux[a]	rms[b]
J0850+5159	2007 Nov 06	7.3	64.0	1.2
J0852+3435	2007 Nov 05	7.5	51.2	2.4
	2007 Nov 30	6.9	52.2	1.3
	2008 Mar 08	6.2	50.1	1.3

[a] in units of mJY beam^{-1}
[b] spectral rms in units of mJy beam^{-1} channel^{-1}.

toward AO 0235+164 (Wolfe & Wills 1977; York et al. 2006; Junkkarinen et al. 2004; Kulkarni et al. 2007). This system also shows strong 21-cm absorption (Wolfe & Wills 1977) and has N(H I) = 5×10^{21} cm^{-2}, E(B-V) = 0.23 (Junkkarinen et al. 2004) and T_s = 220±60 K. Wang et al. (2004) have reported the detection of the 2175Å absorption bump in 3 intermediate redshift ($z \sim 1.3$) Mg II systems. Recently, Ellison et al. (2008) have detected DIBs in the z_{abs}= 0.1556 Ca II systems towards SDSS J001342.44-002412.6. Composite spectra have been obtained for different samples of absorbers from the Sloan Digital Sky Survey (SDSS). They show in a statistical way that dust is present in strong Mg II (York et al. 2006a) and Ca II systems (Wild, Hewett & Pettini 2006). In the former case the mean extinction curve is similar to the SMC curve with a rising ultraviolet extinction below 2175 Å with E(B−V)≤0.08 and with no evidence of an UV bump. In the latter case, evidence for the UV bump is marginal and LMC extinction curve provides E(B-V)≤0.103 for different sub-samples.

An efficient way to reveal cold and dusty gas is to search for 21-cm absorption as shown by the high detection rate of 21-cm absorption towards red QSOs (Carilli et al. 1998; Ishwara-Chandra, Dwarakanath & Anantharamaiah 2003; Curran et al. 2006). Multiple lines of sight toward lensed QSOs passing through regions producing high extinction also show 21-cm and molecular absorption lines (see Wiklind & Combes 1996).

We have recently completed a systematic search for 21-cm absorption in a complete sample of 38 Mg II systems, drawn from the SDSS DR5, with redshifts in the range $1.10 \leq z \leq 1.45$ corresponding to the frequency coverage of 610 MHz feed at GMRT (see Gupta et al. 2007 for early results). Using an automatic procedure we have identified 5 systems in this sample showing strong absorption lines from Si II, Zn II, Cr II, Fe II, Mg II and Mg I in front of radio-loud QSOs with flux density ≥ 50 mJy. Here, we report the detection of 21-cm absorption from two of these systems at z_{abs}∼1.3 towards red (u-K≥4.5 mag) QSOs. The optical spectra of these two quasars possess 2175Å dust absorption features.

2 OBSERVATIONS AND ANALYSIS:

We observed J085042.21+515911.7 (called J0850+5159) and J085244.74+343540.5 (called J0852+3435) with the GMRT to search for 21-cm absorption associated with the Mg II systems at z_{abs}= 1.3265 and z_{abs}= 1.3095 respectively. Log of our observations is presented in Table 1. We used 1 MHz baseband bandwidth split into 128 frequency channels (corresponding to a velocity resolution of ∼3.8 km s^{-1}) centered around the redshifted 21-cm frequency. We observed standard flux density calibrators 3C 147 and 3C 286 every 2-3 hours to correct for amplitude and bandpass variations. Phase calibrators (J0834+555 for J0850+5159 and J0741+312 for J0852+3435) were also observed approximately every 40 min. Data were acquired in both the circular polarization channels, RR and LL and reduced in the standard way using the Astronomical Image Processing System (AIPS) as described in Gupta et al. (2006). GMRT spectra of both sources show detectable 21-cm absorption (see Fig. 1). The broad absorption produced by the z_{abs}= 1.3095 system towards SDSS J0852+3435 is confirmed by repeated GMRT observations obtained at three different epochs spread over 4 months. We have used the combined spectrum for the analysis presented here. It is usual procedure to decompose the absorption profile into multiple Gaussian components. For a Gaussian profile the H I column density and the peak optical depth (τ_p) are related by,

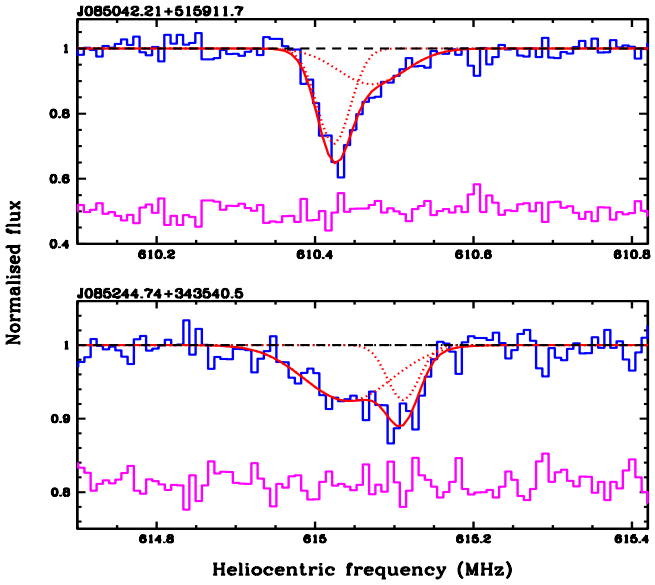

Figure 1. GMRT spectra of J085042.21+515911.7 (top panel) and J085244.74+343540.5 (bottom panel). H I 21-cm absorption is detected at z_{abs} = 1.3265 and 1.3095 (see Table 2), respectively. The solid lines represent the fits to the overall profiles. Individual Gaussian components are shown with dotted lines. Residuals, on a scale arbitrarily shifted for clarity, are also plotted.

Table 2. Details of multiple Gaussian fits to 21-cm absorption lines.

QSO	z_{abs}	Δv^a	τ_p	N(H I) $\frac{f_c^b}{T_s}$
J0850+5159	1.32674	49±16	0.117±0.036	1.11±0.50
	1.32692	24±4	0.347±0.108	1.61±0.57
J0852+3435	1.30919	23±7	0.078±0.025	0.35±0.15
	1.30945	63±12	0.079±0.009	0.96±0.21

[a] FWHM in km s^{-1}; [b] in units of 10^{19} cm^{-2} K^{-1}

Table 3. Rest equivalent widths of UV absorption lines.

Species	Rest equivalent widths (Å)		
	J0850+5159	J0852+3436	Ca II
	$z_{\rm abs}$=1.3265	$z_{\rm abs}$=1.3095	composite
Ca IIλ3934	....	1.05	0.49−1.01
Si IIλ1808	0.96	1.06	....
Mg IIλ2798	4.62	2.89	2.19−2.47
Mg IIλ2803	4.15	2.80	2.07−2.23
Mg Iλ2853	2.08	1.11	0.72−0.93
Mn IIλ2576	0.91	1.25	0.20−0.40
Mn IIλ2594	0.43	1.30	0.15−0.23
Mn IIλ2606	0.50	0.63	0.10−0.12
Fe IIλ2249	0.58	< 0.56	0.09−0.10
Fe IIλ2260	0.55	< 0.56	0.08−0.08
Fe IIλ2344	1.61	1.46	1.36−1.39
Fe IIλ2374	1.72	1.47	0.89−1.01
Fe IIλ2382	2.19	2.36	1.55−1.61
Fe IIλ2586	1.69	1.60	1.27−1.35
Fe IIλ2600	2.27	2.10	1.60−1.80
Zn II+Mg Iλ2026	0.98	0.85	0.12−0.27
Cr IIλ2056	0.67	< 0.30	0.09−0.11
Cr II+Zn IIλ2062	1.12	1.20	0.11−0.20
Cr IIλ2066	0.50	0.39	0.08−0.08
Ti IIλ1910	< 0.10	< 0.20	....
Ti IIλ3242	0.33	0.60	0.09−0.12
Ti IIλ3385	0.63	0.71	0.09

Table 4. Results of SED fitting to the SDSS spectrum.

Object	$z_{\rm em}$	Dust model	A_{V_a}	χ^2_ν
J0850+5159	1.89	MW	0.83(0.06)[1]	2.75
		SMC	0.59(0.05)[1]	1.42
			0.51(0.04)[2]	1.60
			0.51(0.04)[3]	1.36
		LMC2	0.83(0.06)[1]	1.16
			0.73(0.05)[2]	1.43
			0.70(0.05)[3]	1.27
J0852+3435	1.65	MW	1.20(0.08)[1]	2.49
		SMC	0.75(0.06)[1]	2.09
			0.64(0.05)[2]	2.14
			0.68(0.06)[3]	1.99
		LMC2	1.10(0.08)[1]	1.42
			0.95(0.08)[2]	1.64
			0.97(0.08)[3]	1.53

[1] using the SDSS QSO composite spectrum (Vanden Berk et al. 2001); [2] using the HST QSO composite spectrum (Zheng et al. 1997); [3] using LBQS QSO composite spectrum (Francis et al. 1991).

$$N({\rm HI}) f_{\rm c} = 1.93 \times 10^{18}\ \tau_{\rm p}\ T_{\rm s}\ \Delta v\ {\rm cm}^{-2}. \quad (1)$$

Here, Δv and $f_{\rm c}$ are the FWHM (in km s^{-1}) of the fitted Gaussian component, and the covering factor of the absorbing cloud respectively. Results of the Gaussian fits to the 21-cm absorption lines are given in Table 2.

Optical spectra of the QSOs were downloaded from the SDSS archive. In Table 3 we summarize the rest equivalent widths of various metal absorption lines in the two absorption systems and compare them with the range of equivalent widths observed for the Ca II systems by Wild, Hewett & Pettini (2006). A glance at this table suggests that the two systems discussed here have much stronger absorption lines than those associated with the Ca II systems.

Next we compute the extinction due to the Mg II system by assuming the reddening of the quasar to be a consequence of the presence of dust at $z_{\rm abs}$. The optical depth at an observed wavelength λ can be written as,

$$\tau(\lambda) = 0.92 A_{\lambda_{\rm a}} = 0.92 A_{V_a} \xi(\lambda_a). \quad (2)$$

Here, $A_{\lambda_{\rm a}}$ and A_{V_a} are the extinction in magnitude at $\lambda_{\rm a} = \lambda/(1+z_{\rm abs})$ and at the rest V band of the absorber respectively. $\xi(\lambda_a)$ is the relative extinction at $\lambda_{\rm a}$ to that in the rest V band. We consider $\xi(\lambda)$ for the SMC, the LMC2 Supershell and the Galaxy (Misselt, Clayton & Gordon 1999; Gordon et al. 2003) in order of increasing UV bump strength.

We have developed a robust χ^2 minimization code using the IDL routine MPFIT[1] that uses Levenberg-Marquardt technique to get best fit values of $A_{V_{\rm a}}$ and normalization of the flux scale compared to the composite spectrum. We use LBQS, HST and SDSS QSO composite spectra given in Francis et al. (1991), Zheng et al. (1997) and Vanden Berk et al. (2001) respectively. First we shift the composite spectrum to the QSO emission redshift. For each extinction curve we predict the reddened QSO spectrum by multiplying the shifted composite spectrum by $\exp[-\tau(\lambda)]$. We mask the wavelength ranges of strong emission and absorption lines. By varying the flux normalization and A_{V_a} (or E(B-V)) we match the observed spectrum with our model reddened spectrum (see Fig. 2). Results of our best fit models with different extinction curves and associated reduced χ^2 are summarised in Table 4. The error in A_{V_a} includes the effect of errors in the parameters of the extinction curve. For both the systems the lowest value of χ^2 is obtained for the dust extinction models with the extinction curve of LMC2-Supershell irrespective of our choice of composite spectrum.

3 DISCUSSION ON INDIVIDUAL SYSTEMS

3.1 The $z_{\rm abs} = 1.3265$ absorption system towards J085042.21+515911.7

The spectrum of this QSO (with u-K ∼ 4.8 mag) shows a curvature around 2175 Å in the rest frame of the Mg II system (see top panel of Fig. 2). The Milky Way extinction curve that fits the 2175 Å feature over predicts the QSO flux below 4500 Å. This is also the case (not shown in Fig. 2) when we use the average LMC extinction curve. The SMC extinction curve that fits the observed spectrum around 5500 Å under predicts flux below 4500 Å. The LMC2 extinction curve that has a shallow UV-bump and relatively high extinction at rest wavelength $\lambda_r < 2100$ Å compared to that of the Milky Way (and of the LMC) reproduces the data better. We also fitted the spectra of ∼ 200 non-BAL QSOs with $z_{\rm em}$ =1.892±0.005 using SMC extinction curve and find the probability of the 2175 Å feature being produced by QSO-to-QSO spectral variation to be ≤0.03. For

[1] details of MPFIT IDL routine can be found from http://cow.physics.wisc.edu/∼craigm/idl/fitting.html

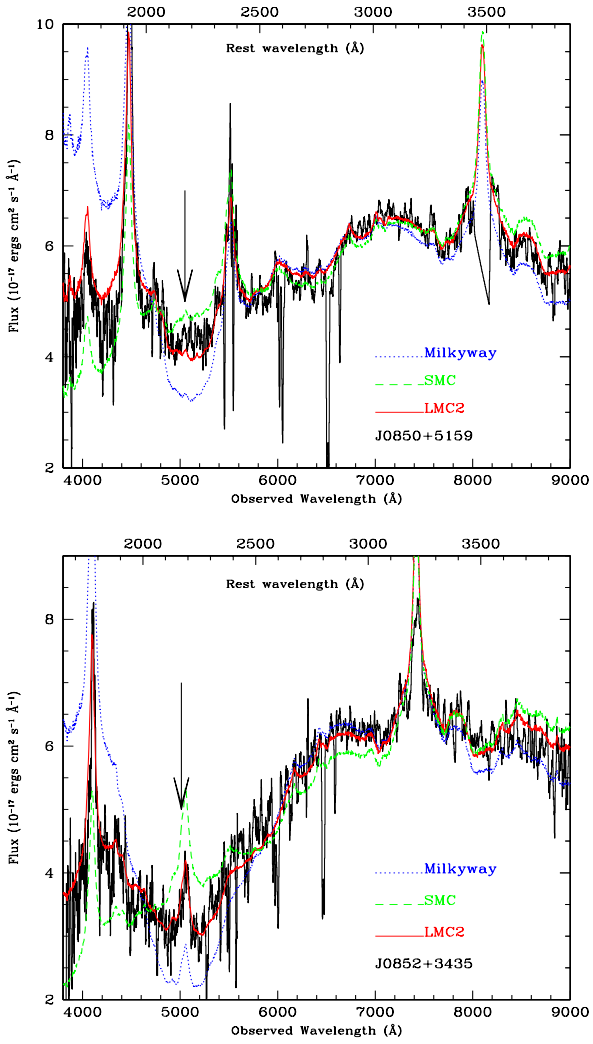

Figure 2. The SDSS spectrum of J0850+5159 (top) and J0852+3435(bottom) are fitted with SDSS composite spectrum corrected using average extinction curves from the Milky Way (dotted), the LMC2 Supershell (solid) and the SMC (dashed). Rest wavelengths at $z_{\rm abs}$are indicated at the top of the figure. The arrow marks the location of 2175 Å feature at $z_{\rm abs}$. For presentation purpose the observed spectrum is boxcor smoothed by 10 pixels.

the range of composite spectra considered here, the mean A_{V_a} is 0.74±0.07 (and E(B−V) = 0.27). Our best fit model prediction J = 16.7, H = 15.8 and K = 14.7 mag, with a typical uncertainty of 0.2 mag, agrees well with the observed values, J = 16.99±0.23, H = 15.72±0.16 and K = 15.27±0.15, from Strutskie et al. (2006). The excess flux predicted in K band can be mainly attributed to the known host galaxy contribution (∼0.3 mag) in the SDSS composite spectrum (See Vanden Berk et al. 2001) at $\lambda_r > 6000$Å.

From Table 2 of Gordon et al. (2003) we have,

$$N({\rm HI}) \sim \frac{A_{V_a}}{\kappa}(6.97 \pm 0.67) \times 10^{21}{\rm cm}^{-2}. \quad (3)$$

Here κ is the ratio of dust-to-gas ratio in the absorption system to that in LMC. We can use the equivalent widths of weak transitions (Table 3) to estimate the column densities of species and derive the depletion factors onto dust-grains assuming Zn is not depleted: −0.5,−0.9, −1.0, −0.9, and −1.0 for [Si/Zn], [Cr/Zn], [Fe/Zn], [Ti/Zn], and [Mn/Zn] respectively. Note that Zn IIλ2062 is blended with a Cr II absorption but we can remove the contribution from Cr II by using the average N(Cr II) derived from unblended lines. Depletion is higher than what is typically seen in high-z absorption systems and are intermediate between what is seen in the Cold and Warm phases in the Galactic ISM (Welty et al. 1999). Clearly more than 90% of the refractory metals are in dust as in the LMC. If we assume $\kappa \sim 0.9$ then we get N(H I) = (5.73±1.10)×10^{21} cm^{-2}.

Our GMRT spectrum shows very strong absorption that can be modelled with two Gaussian components (see Table 2 and upper panel in Fig. 1). The radio spectrum of this source is flat and VLBA maps at 5 and 15 GHz show that more than 90% of the flux density is in the unresolved core (Taylor et al. 2005). Using $f_{\rm c} = 0.9$ in Eq. 1, we derive N(H I) = 3.02±0.84 × 10^{19} $T_{\rm s}$ cm^{-2}. From the total N(H I) inferred from extinction we can estimate the spin temperature, $T_{\rm s} \sim 190^{+124}_{-69}$ K. Note that this value is an upper limit as the dust-to-gas ratio may be larger than 1. All this is consistent with the system being associated with a cold neutral medium with dust properties similar to that seen in LMC2 supershell sample of Gordon et al. (2003).

3.2 The $z_{\rm abs} = 1.3095$ absorption system towards J085244.74+343540.5

This QSO has u-K∼5.6 mag and shows a curvature around 2175 Å in the rest frame of the Mg II system (see bottom panel of Fig. 2) that is stronger than for the previous quasar. The Mg II system at $z_{\rm abs}$= 1.3095 shows absorption lines that are also stronger than that of the previous system. The SDSS spectrum of this quasar is also well reproduced when applying a LMC2 like extinction curve to the QSO composite spectrum (with A_{V_a} = 1.00±0.09 and E(B−V) = 0.36). Using spectra of ∼ 330 non-BAL QSOs with $z_{\rm em}$ =1.655±0.005, we find the probability of the 2175 Å feature being produced by QSO-to-QSO spectral variation to be ≤0.001. Our best fit model prediction J = 16.5, H = 15.2 and K = 14.2 mag agrees reasonably with the observed values, J = 16.75±0.14, H = 15.57±0.11 and K = 15.10±0.12, considering the possible uncertainties in the QSO composite spectrum discussed above. We derive lower limits on the column densities using the weaker metal lines. The absence of Cr IIλ2056 and Fe IIλ2249 features together with the high equivalent width of the Zn II+Cr II blend at $\lambda_r = 2062$ Å is consistent with higher depletion factor and higher metallicity in this system. The detection of Ca II absorption strongly supports this conclusion. From the SED fit and assuming $\kappa = 1$ we derive N(H I) = 6.97±1.30 × 10^{21} cm^{-2}. This may well be an upper limit as κ could be larger than 1.

This system, despite having N(H I)κ similar to that in the $z_{\rm abs}$= 1.3265 towards J0850+5159, has a factor of two lower total integrated N(H I) from 21-cm absorption. This source has a flat radio spectrum and is unresolved in the VLA A-array 8.4 GHz image[2] having a resolution

[2] from CLASS (Cosmic Lens All-Sky Survey) and JVAS (Jo-

of 0".255×0".236. However, high resolution (few mas scale) VLBA map is not available for this source. Therefore, while f_c could be close to 1 its exact value is still uncertain. We get a constraint $N(\mathrm{H\ I})f_c/T_s = 1.31 \pm 0.26 \times 10^{19}$ cm^{-2} K^{-1}. By comparing the two N(H I) estimates we derive $T_s/f_c = 536^{+234}_{-88}$ K. As f_c can be less than unity and κ is probably larger than one, the above value is an upper limit for the gas kinetic temperature. This is consistent with the gas being part of a cold neutral medium.

4 DISCUSSION

During our recently completed GMRT survey to search for 21-cm absorption from intermediate redshift ($1.10 \leq z \leq 1.45$) Mg II systems, we discovered two red QSOs with strong $z \sim 1.3$ Mg II absorption systems along the line of sight. The observed spectral energy distribution of these QSOs are consistent with the QSO spectrum being reddened by dust in the intervening Mg II systems. We fitted the SDSS spectrum using three QSO SDSS composite spectra reddened by different extinction curves. We find that the dust properties of the absorbers are similar to what is seen in the LMC2 supershell. In particular, we detect the 2175 Å UV extinction bump in both individual spectra. The neutral hydrogen column densities, N(H I), inferred from the extinction are consistent with the absorbing gas being of high column density (i.e log N(H I)∼21.7). We used weak metal absorption lines to estimate the column densities of ions of different species. Inferred metallicities are consistent with near solar values and depletion factors are similar to what is measured in the Cold Neutral Medium of LMC.

These two quasars are rather weak (∼ 50 mJy) in radio emission and are not ideally suited for 21-cm absorption observations. We nonetheless detect 21-cm absorption from both systems thanks to the favorable physical conditions in the absorbing gas. These are the first detections of 21-cm absorption at high-z towards such faint background sources. The inferred spin temperatures in these systems are consistent with that of a cold neutral medium gas.

The metal line equivalent widths and E(B-V) about 0.3 measured in the two systems discussed here are higher than those derived from the SDSS composite spectra of Mg II and Na I absorption systems (see York et al. 2006a; Wild, Hewett & Pettini 2006). The E(B-V) values are also higher than the median E(B-V) found for star forming galaxies at $z = 2-3$ and a factor of 2 less than that measured in submillimeter-selected galaxies (see Figure 15 of Wild, Hewett & Pettini 2006). The dust content and N(H I) in the two systems discussed in this paper are comparable to that observed in the 21-cm system toward AO 0234+164. Thus these two systems are ideally suited for high resolution spectroscopic investigation of physical conditions in the interstellar medium of the corresponding absorbing galaxies.

drell/VLA Astrometric Survey) archive website
http://www.jb.man.ac.uk/research/gravlens/class/gmodlist.html

5 ACKNOWLEDGEMENTS

We thank the referee for very useful comments, Rajaram Nityananda for encouragement, and GMRT staff for their cooperation during the observations. The GMRT is an international facility run by NCRA-TIFR. We acknowledge the use of SDSS spectra from the archive (http://www.sdss.org/). RS and PPJ gratefully acknowledge support from the Indo-French Centre for the Promotion of Advanced Research.

REFERENCES

Carilli, C. L., Menten, K. M., Reid, M. J., Rupen, M. P., Yun, M. S. 1998, ApJ, 494, 175
Curran S. J., Whiting M. T., Murphy M. T., Webb J. K., Longmore S. N., Pihlström, Y. M., Athreya, R., Blake, C. 2006, MNRAS, 371, 431
Ellison S., York B. A., Murphy M. T., Zych B. J., Smith A. M., Sarre P. 2008, MNRAS, 383, L30.
Francis P., Hewett P. C., Foltz G., Chaffee F. H.,Weymann R. J., Morris S. L. 1991, ApJ, 373, 465
Gordon, K. D., Clayton, C. G., Misselt, K. A., Landolt, A. U., Wolff, M. J. 2003, ApJ, 594, 279
Gupta N., Salter C. J., Saikia, D. J., Ghosh, T., Jeyakumar, S. 2006, MNRAS, 356, 1509
Gupta N., Srianand R., Petitjean P., Khare P., Saikia D. J., York D. 2007, ApJL, 654, L111
Heng, K. et al., 2008, astrop-ph/0803.2879v2
Ishwara-Chandra C. H., Dwarakanath, K. S., Anantharamaiah K. R. 2003, JAA, 24 37.
Junkkarinen, V. T., Cohen, R. D., Beaver, E. A., Burbidge, E. M., Lyons, R. W. Madejski, G. 2004, ApJ, 614, 658
Kulkarni, V. P., York, D. G., Vladilo, G., Welty, D. 2007, ApJL, 663, 81
Ledoux, C., Petitjean, P., Srianand, R. 2003, MNRAS, 346, 209
Misselt, K.A., Clayton, C. G., Gordon, K. D. 1999, ApJ, 515, 128
Noll, S., Pierini, D., Pannella, M., Savaglio, S. 2007, A&A, 472, 465
Noterdaeme P., Ledoux C., Petitjean P., Srianand R. 2008, A&A, 481, 327
Pettini M., Smith L.J., Hunstead D. L., 1994, ApJ, 426, 79
Petitjean P., Ledoux C., Noterdaeme P., Srianand R. 2006, A&A, 456, L9
Skrutskie, M. F., et al. 2006, AJ, 131, 1163
Srianand, R., Petitjean, P., Ledoux, C., Ferland, G., Shaw, G., 2005, MNRAS, 362, 549
Taylor, G. B. et al. 2005, ApJS, 159, 27
Vanden Berk, D. et al. 2001, AJ, 122, 549
Wang J., Hall P. B., Ge J., Li A., Schneider D. P. 2004, ApJ, 609, 589
Welty D., Frisch P. C., Sonneborn G., York D. G. 1999, ApJ, 512, 636
Wiklind T., Combes F. 2006, Natur, 379, 139
Wild V., Hewett P., Pettini, 2006, MNRAS, 367, 211
Wolfe A.M., Wills B. J. 1977, ApJ, 218, 39.
Wolfire M. G., McKee C. F., Hollenbach D., Tielens A. G. G. M., Bakes E. L. O. 1995, ApJ, 443, 152.
York B. A., Ellison S. L., Lawton B., Churchill C. W., Snow T. P., Johnson R. A., Ryan S. G. 2006, ApJL, 647, 29
York D. G., et al. 2006a, MNRAS, 367, 945
Zheng W., Kriss G. A., Telfer R. C., Grimes J. P., Davidsen A. F. 1997, ApJ, 475, 469.